A Facile Block Copolymer Inclusion Technique for Large Scale Monodisperse Hexagonal Arrays of Superparamagnetic Iron Oxides Nanodots

T. Ghoshal,[*] T. Maity,[**] J. F. Godsell,[**] S. Roy[**] and M. A. Morris[*,***]

[*]Materials Research Group, Department of Chemistry and Tyndall National Institute, University College Cork, Cork, Ireland, g_tandra@yahoo.co.in
[**]Micropower-Nanomagnetics group, Tyndall National Institute, Cork, Ireland
[***]Centre for Research on Adaptive Nanostructures and Nanodevices (CRANN), Trinity College Dublin, Dublin, Ireland

ABSTRACT

We demonstrate a simple, cost-effective route to prepare high density ordered array of iron oxides nanodots based on block copolymer patterning. The methodology creates hexagonally arranged features via a process of selective block copolymer inclusion and allows dimensional and structural control of both features and patterns at large scale. Microscopic and spectroscopic techniques confirmed the uniformity, size monodispersity and same structural arrangement as that of parent block copolymer template. These well-isolated array of nanodots exhibits superparamagnetism. Thermal stability and strong adherence to the substrate surface makes them useful for technological applications.

Keywords: Block copolymer, array, nanodot, superparamagnetism

1. INTRODUCTION

Continued advances in technologies such as magnetic storage and optoelectronics depend critically on the ability to produce highly dense arrays of nanoscaled materials [1-5]. For potential applications of magnetic nanomaterials controlling size of the nanoparticle is considered to be a predominant factor in defining their efficacy. This is of particular relevance to superparamagnetism since, the magnetic properties and their variation with temperature is highly dependent on size as well as interparticle separation. Superparamagnetic nanoparticles have potential applications in areas such as ferrofluids, color imaging, magnetic refrigeration, labelling and sorting of cells, anti-cancer drugs and magnetic resonance imaging (MRI) contrasting agent [6-8]. These applications generally also require chemically stable, uniform size, well dispersed nanoparticles. Whilst there have been numerous reports of the synthesis of nanoparticles, challenges remain on controlling size dispersity and how they may be placed on or in a material with controlled separation (since particle aggregation in dry or solvent environments is common[9]).

To fabricate patterned magnetic nanostructure, a top-down lithographic approach using UV light, electron beam, optical interference, X-ray lithography or nanoimprint lithography can be employed although they are not cost effective [10-11]. Alternatively, bottom up self-assembling techniques using diblock copolymer (DBCP) microphase separation can be used [12-13]. Whilst related preparation techniques are available using BCP micelle methodology which not only involves complex co-ordination chemistry to create iron oxide arrays, but also the products have been seldom characterised in terms of their phases and magnetism [14-15]. DBCP that form cylindrical are particularly interesting because selective removal of the minor component creates nanoporous thin film to generate ordered array of inorganic nanoparticles [16-17]. Here, we have applied a simple methodology to produce long range ordered iron oxides nanopatterns, based on solvent-induced microphase separation in PS-b-PEO thin films which have controlled structure orientation [18] and exploits the marked difference in the chemical selectivity of PS and PEO to allow selective metal ion inclusion [19]. Using the techniques developed here, we were able to generate superparamagnetic patterns with controllable sizes of the nanodots over wafer scale areas. The methodology avoids the need to remove a selected component of the DBCP. Further the technique avoids the use of sol-gel or other infill methods [20]. The methodology also uses a UV/ozone treatment to convert the DBCP-inorganic component combination into a rigid oxide pattern and is effective because of its ability to converting non-volatile inorganic compounds into oxides whilst removing organic components [21].

2. EXPERIMENTAL

Polystyrene-b-poly(ethylene oxide) (PS-b-PEO) diblock copolymer was purchased from Polymer Source (number-average molecular weight, M_n, PS =

42 kg mol^{-1}, M_n, PEO = 11.5 kg mol^{-1}, M_w/M_n = 1.07, M_w: weight-average molecular weight). PS-b-PEO was dissolved in toluene to yield 0.9 wt% polymer solution at room temperature. The PS-b-PEO thin film was formed by spin coating the polymer solution (3000 rpm for 30 s). The film was exposed to toluene/water (50:50, v/v) mixed vapour placed at the bottom of a closed vessel kept at 50^{0}C for 1h under static vacuum. The film was immersed in ethanol at 40 ^{0}C for 15 h to obtain the activated thin film. Different concentration iron (III) nitrate nonahydrate ($Fe(NO_3)_3$,$9H_2O$) was dissolved in ethanol and spin-coated onto the activated film. UV/Ozone treatment was used to oxidize the precursor and remove polymer.

Surface morphologies were imaged by scanning probe microscopy (SPM, Park systems, XE-100) and scanning electron microscopy (SEM, FEI Company, FEG Quanta 6700). The film thicknesses were measured by optical ellipsometer (Woolam M2000). X-Ray photoelectron spectroscopy (XPS) experiments were conducted on a Thermo K-alpha machine with Al K_α X-ray source operating at 72 W. The magnetic properties of the samples were investigated using a Superconducting Quantum Interference Device (Model: Quantum Design MPMS-XL5).

3. RESULTS AND DISCUSSION

3.1 Structural characterization

A schematic diagram of the fabrication process is described in Scheme 1.

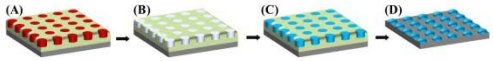

Scheme 1. Schematic illustration of the fabrication of iron oxides nanodots. (A) Highly ordered PS-b-PEO thin film prepared by solvent annealed process. (B) Nanoporous template produced by activation of PEO cylinders. (C) iron oxide precursor moves into the cylinders after spin coating the precursor solution. (D) iron oxide dots remain after UV/Ozone treatment.

The as-coated PS-b-PEO thin films exhibit mixed orientation of PEO cylinders i.e. parallel and perpendicular orientation with respect to the substrate, without any sign of long-range ordering. Solvent annealing in a mixed toluene/water environment was used to induce long range-ordering. The resultant film is of regular thickness with no signs of de-wetting and is well-ordered across the entire substrate. Figure 1a shows an AFM image of the film (40 nm thick as determined by ellipsometry) with PEO cylinders seen in the darker colour. The measured average centre-to-centre cylinder spacing is 42 nm with a PEO cylinder diameter of 19.3 nm. The strong multiple peaks in the FFT pattern shown in the inset of Figure 1a confirm a highly ordered hexagonal arrangement of PEO cylinders. The SEM image in Figure 1b also depicts long range ordering of the PS-PEO thin film.

When the solvent annealed films were ethanol treated at 40^{0}C for 15 h, modification of the film occurred although the structural arrangement and dimensions are unchanged. The AFM image (Figure 1c) shows some increase in the phase contrast and an increase in long-rage order. This is also indicated by the Fourier transform of the AFM image (inset of Figure 1c) where six-point patterns with multiple higher order reflections are shown, characteristic of exceptional long-range order. Also, the SEM image contrast was enhanced by ethanol exposure as seen in Figure 1d. No thickness loss was observed after the ethanol treatment as measured by optical ellipsometery. The ethanol treatment is a pre-requisite to form well-defined oxide nanopatterns in later steps and is described as an 'activation step'.

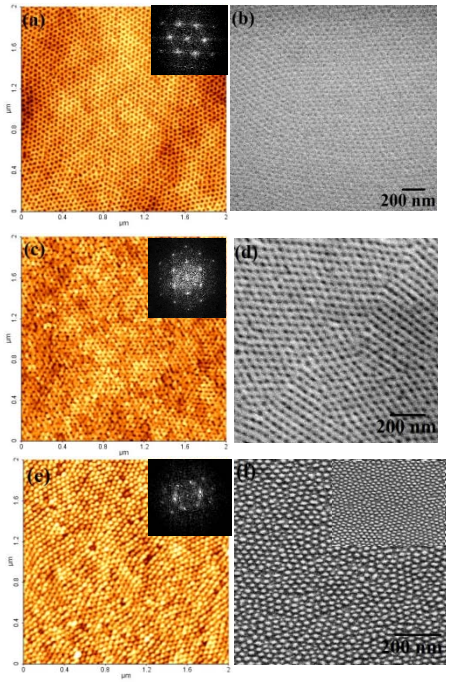

Figure 1. Atomic force microscoy (AFM) and Scanning electron microscopy (SEM) images of (a, b) PS-b-PEO thin film (c, d) Nanoporous template after ethanol treatment (e, f) iron oxide nanodots formed after UV/Ozone treatment. Insets of a, c and e shows the corresponding FFT pattern. Inset of f shows iron oxide nanodots annealed at 800^{0}C for 1h.

Oxide nanodots are formed by simple inclusion of metal ions (iron nitrate ethanol solution) into the PEO component. Considering the fact that the spin coating

was performed for just a few seconds, diffusion through the pores and enrichment of the solid inside the pores must be a rather rapid process. After iron ion inclusion, UV/ozone treatment was carried out immediately so as to remove any solvent, oxidizes and cross-linking iron ions forming oxide and remove the organic part simultaneously. Figure 1e and f shows the AFM and SEM images of well-ordered iron oxide nanodots (0.4 wt% iron nitrate ethanol solution) formed after the UV/ozone treatment. The structural arrangement remains unchanged. FFT pattern shown in the inset of Figure 1e confirms the hexagonal ordering of the nanodots. This confirms that these have been produced via direct templating of the PS-b-PEO film. The average diameter of the nanodots is 24 nm and the height measured by ellipsometry is 9 nm. The density of the nanodots on the substrate was approximately 4.2 x 10^{10} nanodots cm^{-2}. The iron oxide nanodots are well-adhered to the substrate and thermally robust. Typical data is presented in the inset of Figure 1f which shows iron oxide nanodots after air calcination at 800^0C for 1 h, revealed the ordered structure of the nanodots. The only effect of heating was a reduction in the average diameter and height consistent with high temperature densification.

3.2 Composition and phase by XPS

XPS was used to confirm the crystalline phase and surface composition of the substrate after UV/Ozone treatment and further calcination. Figure 2 shows the survey spectrum indicating presence of expected elements, Si, O, Fe and a small C1s (~285 eV) feature due to adventitious carbon. High resolution Fe2p spectra (pass energy = 20 eV) were recorded to distinguish different phases of iron oxides. Fe 2p core level spectrum recorded on iron oxide nanodots prepared after UV/Ozone treatment (inset of Figure 2, left) consists of two peaks associated with Fe $2p_{3/2}$ at 711 eV and Fe $2p_{1/2}$ at 724.4 eV and broadened due to the existence of Fe^{+2} and Fe^{+3} ions. The Fe $2p_{3/2}$ and Fe $2p_{1/2}$ binding energies (BEs) for Fe^{+2} and Fe^{+3} were determined by curve-fitting using Gaussian-Lorentzian line shapes. The measured Fe $2p_{3/2}$ and Fe $2p_{1/2}$ BEs are 709.7 and 723 eV (assigned to Fe^{+2}) and 711.6 and 725 eV (Fe^{+3}) matches literature values [22]. The concentration ratio of Fe^{+3}/ Fe^{+2} was calculated from the curve-fitted peak areas as about 2:1 as expected for Fe_3O_4. Fe 2p core level spectrum of iron oxide nanodots after calcination (inset of Figure 2, right) consists of two sharp peaks associated with Fe $2p_{3/2}$ and Fe $2p_{1/2}$ at 711.3 and 725.1 eV accompanied by high binding energy satellite structures (+8 eV shift). These data are consistent with the existence of Fe^{+3} (Fe_2O_3) ions only [23-24]. Thus, XPS analysis confirms the formation of phase pure iron oxides without any polymer residues.

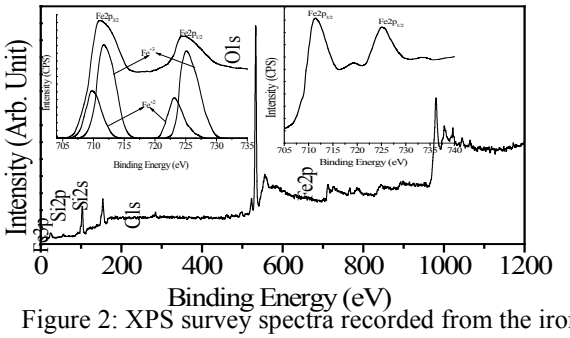

Figure 2: XPS survey spectra recorded from the iron oxide nanodots on Si substrate. Insets shows high resolution spectrum for Fe 2p core level revealed Fe_3O_4 (left) and Fe_2O_3 (right) phase.

3.3 Feature size variation

The diameter and height of the nanodots can be varied by varying the concentration of precursor solution without changing their structural arrangement. As shown in Figures 3a, b and c, well ordered arrays of iron oxide nanodots with average diameters 18, 24 and 30 nm were generated from 0.3, 0.4 and 0.5 wt% iron nitrate-ethanol solution respectively. It should be noted that metal ion solution concentrations exceeding 1% result in the deposition of localised agglomerated 3D nanoparticle structures across the substrate surface.

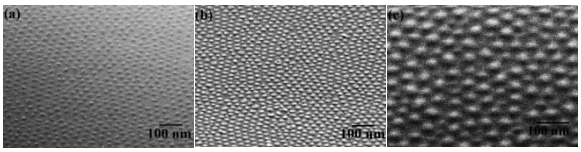

Figure 3: SEM images of iron oxide nanodots for different concentrations of precursor.

3.4 Magnetic properties

The magnetic properties of these two different iron oxide nanodots assemblies on quartz crystal substrate were studied and found to be consistent superparamagnetism. Figure 3a (inset) and 3b (inset) show the temperature dependence of typical field cooled (FC) and zero field cooled (ZFC) magnetization measured with an applied magnetic field of 100 Oe from 300 K to 2 K for ordered arrays of Fe_3O_4 and Fe_2O_3 nanodots respectively. For Fe_3O_4, the FC curve shows a clear deviation from the ZFC magnetization curve which shows a maximum at 180 K, the blocking temperature of Fe_3O_4 nanodots. For Fe_2O_3 (calcined sample) the maximum magnetization and subsequent decrease in the ZFC curve are

observed at 100K which determines the Fe_2O_3 nanodot blocking temperature.

The superparamagnetic character of the nanodots is confirmed by magnetic hysteresis measurements at temperatures below (T~2 K) and above (T~300 K) the blocking temperature. Above the blocking temperature the coercivities were could not be measured accurately but could be estimated as < 20 Oe. At 2K, the coercivity for Fe_3O_4 nanodots is much higher (~975 Oe) than that of Fe_2O_3 (~235 Oe). These data are consistent with the production of single crystal nanodots that are uniform in size and well dispersed at a substrate surface.

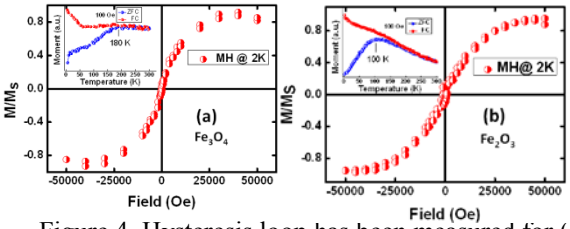

Figure 4. Hysteresis loop has been measured for (a) Fe_3O_4 and (b) Fe_2O_3 nanodots array on quartz substrate. Magnetization as a function of temperature in the applied field of 100 Oe between 2 to 300 K using field cooling (FC) and zero-field cooling (ZFC) procedures (insets). For the sake of presentation, we have normalized (M/M_S) the magnetization data for MH curve and relative change in FC-ZFC has been shown in arbitrary unit.

4. CONCLUSION

In conclusion, this technique is a simple and cost-effective route for fabrication of well-ordered arrays of superparamagnetic iron oxides nanodots at substrate surfaces by block copolymer inclusion. Further, the techniques described are scaleable to wafer scale using spin-coating and simple processing techniques. The nanodots have uniform size and shape and their placement mimics the original self-assembled block copolymer pattern. The nanodots have good thermal stability and strong adherence to the substrate surface. The ability to create nanodots of controlled size by metal ion concentration could provide a very useful means to generate practical device technologies.

*Acknowledgements:*The authors would like to thank Science Foundation Ireland for support of this project through the Strategic Research Cluster FORME grant and the CSET CRANN grant.

REFERENCES

[1] H. G. Craighead; J. Appl. Phys., 1984, 55, 4430.
[2] A. Wiedensohler, H. C. Hansson, I. Maximov, L. Samuelson; Appl. Phys. Lett., 1992, 61, 837.
[3] A. P. Alivisatos; Science, 1996, 271, 933.
[4] H. J. Fan, P. Werner, M. Zacharias; Small, 2006, 2, 700.
[5] Y. Cui, M. T. Bjork, J. A. Liddle, C. Sonnichsen, B. Boussert, A. P. Alivisatos; Nano Lett., 2004, 4, 1093.
[6] K. J. Kim, J. H. Lee, S. H. Lee; J. Magn. Magn. Mater., 2004, 279, 173.
[7] J. Manent, K. Oguievetskaia, J. Bayer, N. Ratner, M. Giovannini; J. Neurosci. Methods, 2003, 123, 167.
[8] C. Alexiou, W. Arnold, R. J. Klein, F. G. Parak, P. Hulin, C. Bergemann, W. Erhardt, S. Wagenpfeil, A. S. Lubbe; Cancer Res., 2000, 60, 6641.
[9] H. N. Cao, J. He, L. Deng, X. Q. Gao; Appl. Surf. Sci., 2009, 255, 7974.
[10] G. M. Wallraff, W. D. Hinsberg; Chem. Rev., 1999, 99, 1801.
[11] F. Rousseaux, D. Decanini, F. Carcenac, E. Cambril, M. F. Ravet, C. Chappert, N. Bardou, B. Bartenlian, P. Veillet; J. Vac. Sci. Technol. B, 1995, 13, 2787.
[12] J. Y. Cheng, C. A. Ross, V. Z. H. Chan, E. L. Thomas, R. G. H. Lammertink,G. J. Vancso; Adv. Mater., 2001, 13, 1174.
[13] M. Park, C. Harrison, P. M. Chaikin, R. A. Register, D. H. Adamson; Science, 1997, 276, 1401.
[14] S. H. Yun, B. H. Sohn, J. C. Jung, W. C. Zin, J. K. Lee, O. Song; Langmuir, 2005, 21, 6548.
[15] B. K. Kuila, M. S. Rama, M. Stamm; Adv. Mater., 2011, 23, 1797.
[16] R. Olayo-Valles, S. W. Guo, M. S. Lund, C. Leighton, M. A. Hillmyer; Macromolecules, 2005, 38, 10101.
[17] T. Thurn-Albrecht, J. Schotter, C. A. Kastle, N. Emley, T. Shibauchi, L. Krusin-Elbaum, K. Guarini, C. T. Black, M. T. Tuominen, T. P. Russell; Science, 2000, 290, 2126.
[18] P. Mokarian-Tabari, T. W. Collins, J. D. Holmes, M. A. Morris; ACS Nano, 2011, 5, 4617.
[19] D. Kannaiyan, E. Kim, N. Won, K. W. Kim, Y. H. Jang, M. A. Cha, D. Y. Ryu, S. Kim, D. H. Kim; J. Mater. Chem., 2010, 20, 677.
[20] J. Peng, X. Li, D. H. Kim, W. Knoll; Macromol. Rapid Commun., 2007, 28, 2055.
[21] M. Ouyang, C. Yuan, R. J. Muisener, A. Boulares, J. T. Koberstein; Chem. Mat., 2000, 12, 1591.
[22] R. Prakash, R. J. Choudhary, L. S. S. Chandra, N. Lakshmi, D. M. Phase; J. Phys.-Condes. Matter, 2007, 19.
[23] P. Mills, J. L. Sullivan; J. Phys. D-Appl. Phys., 1983, 16, 723.
[24] T. Fujii, F. M. F. de Groot, G. A. Sawatzky, F. C. Voogt, T. Hibma, K. Okada; Physical Review B, 1999, 59, 3195.